Microchemical Journal 137 (2018) 51–61

Contents lists available at ScienceDirect

Microchemical Journal

journal homepage: www.elsevier.com/locate/microc

Direct analysis of benzo[*a*]pyrene metabolites with strong overlapping in both the spectral and lifetime domains

Bassam Alfarhani [1], Maha Al-Tameemi, Hector C. Goicoechea [2], Fernando Barbosa Jr [3], Andres D. Campiglia *

Department of Chemistry, 4000 Central Florida Blvd., Physical Sciences Room 211, University of Central Florida, Orlando, FL 32816-2366, United States

ARTICLE INFO

Article history:
Received 12 June 2017
Received in revised form 21 September 2017
Accepted 21 September 2017
Available online 23 September 2017

Keywords:
Solid-phase extraction
Time-resolved excitation emission matrices
Urine analysis
UPLS/RTL
PAH metabolites

ABSTRACT

The ultimate goal of the present study is to develop screening methodology for the urine analysis of metabolites of polycyclic aromatic hydrocarbons. The investigated approach is based on surface matrix fluorescence spectroscopy, where octadecyl silica membranes serve the dual purpose of metabolite extraction and solid substrate for fluorescence measurements. One of the main challenges faced by this approach is the interference of concomitants in the sample matrix. The present study focuses on three metabolites with strong spectral and lifetime overlapping, namely benzo[*a*]pyrene-*trans*-9,10-dihydrodiol, benzo[*a*]pyrene-r-7,t-8,c-9-tetrahydrotriol and benzo[*a*]pyrene-*r*-7,*t*-8,*c*-9,*c*-10-tetrahydrotetrol. As an attempt to improve spectral and lifetime resolution, time-resolved excitation emission matrices are recorded at 77 K with the aid of a cryogenic fiber optic probe and laser-based instrumentation. In comparison to conventional spectrofluorimeters, the use of laser-based instrumentation improves the limits of detection by approximately two-orders of magnitude. The fiber optic probe facilitates the collection of time-resolved excitation emission matrices for the detection of the three metabolites at the pg mL^{-1} concentration level. Their accurate determination in urine samples of unknwon composition is only possible with the aid of unfolded-partial least squares/residual tri-linearization. This algorithm demonstrated to be well-equipped to handle strong overlapping in both the spectral and time domains.

1. Introduction

Polycyclic aromatic hydrocarbons (PAHs), which comprise a group of compounds featuring two or more aromatic rings containing no other elements than hydrogen and carbon, are important environmental pollutants originating from a wide variety of natural and anthropogenic sources. PAHs are generally formed during incomplete combustion of organic matter containing carbon and hydrogen. Because combustion of organic materials is involved in countless natural processes or human activities, PAHs are omnipresent and abundant pollutants in the environment. Due to the ubiquitous occurrence and extreme eco-toxicological relevance of PAHs, the U.S. Environmental Protection Agency (EPA) and the European Community include sixteen PAHs in their "Priority Pollutants List" with molecular weights ranging from 128 g mol^{-1} (naphthalene) to 278 g mol^{-1} (dibenz[*a*,*h*]anthracene). In order to prevent human exposure to PAHs contamination, the EPA recommends the routine monitoring of the sixteen priority pollutants in air, soil and water samples [1].

Environmental monitoring of PAHs is an important tool in pollution control but it provides limited information on human PAH uptake and subsequent health risks. Parent PAHs are relatively inert and need metabolic activation to express their detrimental health effects. In order to assess the amounts of PAHs adsorbed and metabolized, considerable efforts have been made to develop bio-analytical techniques capable to determine concentration levels of PAH metabolites in urine samples. Urine analysis of PAH metabolites is recognized as an accurate assessment of individual exposure to PAHs contamination. The general scheme consists on sample clean-up and pre-concentration prior to chromatographic separation and determination [2–12].

Although chromatographic techniques provide robust methods for the analysis of PAH metabolites, the assessment of PAHs uptake by large populations calls for straightforward procedures with high sample throughput. Research in our group has focused on the development of solid matrix photoluminescence spectroscopy. Our approach is based on solid-phase extraction (SPE) photoluminescence spectroscopy, an approach originally developed for the determination of organic pollutants in water samples [13–19] and later extended to the analysis of PAH metabolites in urine samples [20–23]. Several features make solid matrix photoluminescence spectroscopy an attractive approach for

* Corresponding author.
E-mail address: andres.campiglia@ucf.edu (A.D. Campiglia).
[1] Present address: Department of Chemistry, College of Sciences, University of Al-Qadisiyah, Diwaniah City, Iraq.
[2] Laboratorio de Desarrollo Analítico y Quimiometría, Catedra de Química Analítica I, Facultad de Bioquímica y Ciencias Biológicas, Universidad Nacional del Litoral, Ciudad Universitaria, 3000, Santa Fe, Argentina.
[3] Laboratório de Toxicologia e Essencialidade de Metais, Faculdade de Ciências Farmacêuticas de Ribeirão Preto, Universidade de São Paulo, Ribeirão Preto, SP, Brazil.

https://doi.org/10.1016/j.microc.2017.09.022
0026-265X/

screening metabolites in urine samples. PAH metabolites are extracted from urine samples with an octadecyl (C-18) silica membrane and determined on the surface of the solid substrate via room-temperature fluorescence (RTF) spectroscopy. Since metabolite quantification does not require elution steps, excellent recoveries (~100%) are often obtained with a straightforward procedure [20–24]. The strong fluorescence from the rigid and delocalized π-electron system of PAH metabolites on C-18 membranes provides SPE – RTF with competitive limits of detection (LODs) at the pg mL^{-1} concentration levels.

The main limitation of SPE-RTF results from the spectral overlapping of co-extracted metabolites and other fluorescence species that might also exist in urine samples of unknown composition. Previous attempts in our lab to improve the selectivity of the technique have combined multidimensional data formats to multiway deconvolution methods. The direct quantification of 1-hydroxynaphthalene, 2-hydroxynaphthalene, 1-hydroxypyrene, 3-hydroxybenzo[*a*]pyrene, 2-hydroxyfluorene and 9-hydroxyphenanthrene in urine samples was made possible by processing RTF excitation-emission matrices (EEMs) [22] or total synchronous fluorescence spectra [23] with unfolded-partial least squares/residual bi-linearization (U-PLS/RBL). Both data formats were generated with the aid of a commercial spectrofluorimeter equipped with a continuous excitation source for steady state spectroscopy.

In this article, we add the temporal dimension to EEMs for the direct analysis of benzo[*a*]pyrene-*trans*-9,10-dihydrodiol (B[*a*]P-diol), benzo[*a*]pyrene-r-7,t-8,c-9-tetrahydrotriol (B[*a*]P-triol) and benzo[*a*]pyrene-*r*-7,*t*-8,*c*-9,*c*-10-tetrahydrotetrol (B[*a*]P-tetrol) in urine samples. Benzo[*a*]pyrene (B[*a*]P) is the most toxic PAH in the EPA priority pollutants list and its metabolites are often used as a measure of risk. The strong overlapping that exists among the spectral features of B[*a*]P-diol, B[*a*]P-triol and B[*a*]P-tetrol illustrates the analytical challenge associated with the heterogeneous distribution of metabolic products of B[*a*]P.

Recall that an EEM can be equivalently viewed as either a series of excitation spectra taken at different emission monitoring wavelengths or a series of emission spectra taken at different excitation wavelengths. The order in which the data are collected isn't relevant; the elements of the EEM are intensities as a function of excitation and emission wavelengths. The third data dimension, fluorescence decay time, doesn't enter into conventional EEMs because the excitation source is continuous. Adding the temporal dimension to EEMs requires the use of a short duration excitation pulse [25,26]. The complete data set – which is known as a time-resolved excitation emission matrix (TREEM) – consists of intensities as a function of excitation and emission wavelengths and delay times after the short duration of the excitation pulse.

The approach we present here is based on the collection of 77 K time-resolved excitation emission cubes (TREECs). This data format refers to the superposition of TREEMs recorded at different time windows from the laser excitation pulse [27]. Spectral deconvolution was carried out with parallel factor analysis (PARAFAC) and unfolded-partial least squares/residual tri-linearization (U-PLS/RTL). The best predication abilities were obtained with U-PLS/RTL. The accuracy of analysis demonstrates the potential of U-PLS/RTL for the direct determination of metabolites with strong spectral overlapping and almost identical time emission windows.

2. Theory

PARAFAC is an algorithm able to model four-way data arrays ($\boldsymbol{X}$) which are obtained by assembling third-order data – such as TREECs - of size J (excitation wavelength) × K (emission wavelength) × L (time) for a set of I calibration samples, whose dimensions are [$(I + 1) \times J \times K \times L$]. For a proper PARAFAC modeling, it is of extreme importance that $\boldsymbol{X}$ follows a quadrilinear structure, which can be represented by Eq. (1) [28]:

$$x_{ijkl} = \sum_{n=1}^{N} a_{in} b_{jn} c_{kn} d_{\ln} + e_{ijkl} \tag{1}$$

where x_{ijkl} is an element of the four-way array, $a_{\ln}$ is the score of component n in sample i, N is the total number of responsive components, b_{jn}, c_{kn} and d_{ln} are the loading elements in the excitation, emission and time dimensions, respectively, and e_{ijkl} is an element of the array of errors not fitted by the model.

The model described by Eq. (1) defines a decomposition of $\boldsymbol{X}$ which provides access to excitation ($\mathbf{B}$) and emission spectral profiles ($\mathbf{C}$), time profiles ($\mathbf{D}$) and relative concentrations ($\mathbf{A}$) of individual components in the $(I + 1)$ samples. Decomposition is usually implemented with an alternating least-squares minimization scheme [29]. Relative concentrations allow performing a pseudo-univariate calibration plot, regressing them vs. the nominal concentrations of standards, in order to predict analyte concentrations in unknown samples by projecting their relative concentration in the mentioned plot.

Unfolded partial-least squares (U-PLS) is an extended version of the first order data PLS algorithm, which makes it possible to operate with higher order data. The cube-structured data for each sample are transformed into vectors by unfolding them. In the calibration step, the concentration information included in the vector $\mathbf{y}$ $(I \times 1)$ is employed, excluding data for the unknown sample [30]. Thus, a set of loadings $\mathbf{P}$ and weight loadings $\mathbf{W}$ ($JKL \times A$, where A is the number of latent variables) as well as regression coefficients $\mathbf{v}$ (size $A \times 1$) arte obtained. The parameter A is usually selected by the well-known leave-one-out cross-validation procedure. Analyte concentrations in unknown samples are predicted with $\mathbf{v}$ using the following equation:

$$y_u = \mathbf{t}_u{}^T v \tag{2}$$

where $\mathbf{t}_{\mathrm{u}}$ (size $A \times 1$) is the unknown sample score, obtained by projection of the (unfolded) data for the test sample vec($\boldsymbol{X}_{\mathrm{u}}$) of size ($JKL \times 1$) onto the space of the A latent factors:

$$\boldsymbol{t}_{\mathrm{u}} = \left(\mathrm{w}^{\mathrm{T}}\boldsymbol{P}\right)^{-1}\boldsymbol{W}^{\mathrm{T}}\mathrm{vec}(X_{\mathrm{u}}) \tag{3}$$

If the sample under evaluation contains unexpected components, the scores given by Eq. (3) will generate abnormally large residuals compared with the typical instrumental noise when the prediction is performed using Eq. (2). Fortunately, the effect of unexpected components in samples can be modelled with the RTL procedure through the Tucker3 decomposition [31]. The latter is performed by minimizing the norm of the residual vector $\mathbf{e}_{\mathrm{u}}$, i.e. s_{u}, computed while fitting the sample data to the sum of the significant contributions to the sample signal. For a single interference, the expression can be formulated:

$$\mathrm{vec}(X_{\mathrm{u}}) = \mathbf{P}\ \mathbf{t}_{\mathrm{u}} + g_{\mathrm{int}}(\mathbf{d}_{\mathrm{int}} \otimes \mathbf{c}_{\mathrm{int}} \otimes \mathbf{b}_{\mathrm{int}}) + \mathbf{e}_{\mathrm{u}} \tag{4}$$

where $\mathbf{b}_{\mathrm{int}}$, $\mathbf{c}_{\mathrm{int}}$ and $\mathbf{d}_{\mathrm{int}}$ are normalized profiles in the three modes for the interference and g_{int} is the first core element obtained for Tucker3 analysis of $\boldsymbol{E}$p in the following way:

$$(g_{\mathrm{int}}, \mathbf{b}_{\mathrm{int}}, \mathbf{c}_{\mathrm{int}}, \mathbf{d}_{\mathrm{int}}) = \mathrm{Tucker3}\ (E_{\mathrm{p}}) \tag{5}$$

The number of interferences N_{i} can be assessed by inspection of the final residuals s_{u} (obtained from $\mathbf{e}_{\mathrm{u}}$ of Eq. 4) as a function of N_{i}, until s_{u} stabilizes at a value that matches the experimental noise.

3. Experimental

3.1. Chemicals and materials

All solvents were Aldrich HPLC grade. All chemicals were analytical-reagent grade and utilized without further purification. Unless otherwise noted, Nanopure water was used throughout. B[*a*]P-diol, B[*a*]P triol and B[*a*]P-tetrol were purchased from Sigma–Aldrich. All other chemicals were purchased from Fisher Chemical. The Sep-Pak C-18 membranes were purchased from Varian/Agilent. The synthetic urine solution was manufactured by RICCA Chemical Company (Arlington, TX) and purchased from Fischer Scientific. Human urine samples obtained from an anonymous volunteer group of healthy non-smoking individuals were pooled, frozen and stored at 4 °C until further analysis.

3.2. Preparation of stock solution of B[a]P metabolites

Stock solutions of B[*a*]P metabolites (100 μg mL^{-1}) were prepared by dissolving 1.0 mg of standards in 10 mL of methanol. All stock solutions were kept in the dark at 4 °C. Prior to use, stock solutions were monitored via RTF spectroscopy for possible photo-degradation of the metabolites. All stock solutions were used within 6 months of preparation. Working solutions of B[*a*]P metabolites were prepared daily by serial dilution of stock solutions.

Calibration experiments were carried out with pure (individual) standard solutions containing each metabolite at the 0.05, 0.25, 0.50 and 1.20 ng mL^{-1} concentration level. Sample preparation for validation studies followed a central composite design with 16 samples of metabolites concentrations ranging from 0.23 to 1.20 ng mL^{-1}. The same design was used for the test samples, which consisted of synthetic and real urine samples spiked with known concentrations of the studied metabolites.

3.3. Hydrolysis of urine samples

Hydrolysis of urine samples followed the procedure reported previously [24]. 8 mL of urine sample were spiked with 1 mL of metabolite stock solution of appropriate concentration and equilibrated for 30 min to allow for the interaction of B[*a*]P metabolites with urine components. Then 500 μL of 0.1 M HCl were added to the sample and the mixture was buffered with 500 μL of 0.05 M potassium biphthalate sodium hydroxide buffer (pH 5.0). The buffered sample was shaken for 30 min at 1400 rpm to allow for urine hydrolysis.

3.4. Fluorescence background treatment of extraction membranes

Reduction of fluorescence background from extraction membranes was accomplished with a TLC procedure previously developed in our lab [20–24]. The background reduction treatment improves the LODs of fluorescence measurements on solid substrates. Each chromatographic run was carried out with 34 mm × 40 mm membrane strips immersed 5 mm deep in methanol for approximately 15 min. Each membrane strip was submitted to 3 chromatographic runs to achieve the minimum fluorescence background possible. Extraction disks were cut from the strip areas with low fluorescence backgrounds, stored in a glass desiccator and protected from light until further use for urine extraction.

3.5. Solid-phase extraction with C-18 membranes

A cork-borer with an inside diameter of 4 mm was used to dissect 47 mm C-18 membranes into 4 mm extraction disks. 4 mm disks were individually loaded into a stainless steel filter syringe kit (Alltech) and then connected to a 10 mL Hamilton syringe. Manual positive pressure forced all liquid solutions through the disk. The optimization of experimental parameters for best retention of B[*a*]P metabolites on extraction membranes led to the following procedure: standard metabolite solutions and urine samples were processed through extraction membranes previously conditioned with 5 mL methanol and 5 mL water. Following sample extraction, each membrane was sequentially rinsed with 5 mL of water and 5 mL of 1% ammonium hydroxide. Void water was mechanically removed from the membrane by 300 mL of air through the disk with the 100 mL syringe. Once the urine sample had been extracted, the membrane was stored in a desiccator for fluorescence measurements at 77 K. Since the fiber optic probe preserves the physical integrity of the sample, the extraction membrane can be repeatedly submitted to fluorescence measurements at liquid nitrogen temperature. However, each membrane should be used only once for urine extraction.

3.6. Fiber optic probe

The fiber optic probe (FOP) for measuring photoluminescence from the surface of SPE membranes has been thoroughly described in previous publications [26,32]. It consists of an assembly with one excitation and six collection fibers fed into a 1.25 m long section of copper tubing that provides mechanical support to lower the probe into the liquid cryogen. All the fibers are 3 m long and 500 μm core diameter silica-clad silica with polyimide buffer coating (Polymicro Technologies, Inc.). At the analysis end, the excitation and emission fibers were arranged in a conventional six-around-one configuration, bundled with vacuum epoxy (Torr- Seal, Varian) and fed into a metal sleeve for mechanical support. The copper tubing is flared stopping a swage nut tapped to allow for the threading of a 0.75 mL polypropylene sample vial. At the instrument end, the excitation fiber is positioned in a straight tip connection and aligned with the beam of the tunable dye laser while the emission fibers are bundled with vacuum epoxy in a slit configuration, fed into a metal sleeve, and aligned with the entrance slit of the spectrometer.

3.7. Measurements with the fiber optic probe

SPE membranes are placed at the bottom of the FOP vial with the aid of tweezers. The FOP is then positioned at an optimum distance from the surface of the membrane for maximum signal intensity. Room temperature measurements are made by placing the FOP in a dark environment. 77 K measurements are made by lowering the FOP into a 3 L liquid nitrogen Dewar.

3.8. Spectrofluorimeter

The initial survey of excitation and emission spectra was conducted with a FluoroMax-3 (Horiba Jobin Yvon, Edison, NJ) equipped with a 450 W xenon arc source. The 1200 grooves/mm gratings in the single excitation and emission monochromators were blazed at 330 and 500 nm, respectively. Their reciprocal linear dispersion was equal to 4.25 nm mm^{-1}. The uncooled photomultiplier tube (Hamamatsu, Model R928) detector was operated in the photon- counting mode. Commercial software (DataMax, version 2.20, Horiba Jobin Yvon) was used for automated scanning and fluorescence data acquisition. The excitation fiber and the emission bundle of the FOP were coupled to the sample compartment of the spectrofluorimeter with the aid of a commercial fiber optic mount (F-3000, Horiba Jobin Yvon) that optimized collection efficiency via two concave mirrors. Position alignment of each end of the FOP with the respective focusing mirror was facilitated using commercially available adapters (Horiba Jobin Yvon) [33]. Unless otherwise noted, all excitation and emission spectra were recorded with a 2 nm excitation and emission band-pass.

3.9. Instrumentation for lifetime analysis and TREEM collection

Fluorescence lifetimes and TREEMs were recorded with the aid of an instrumental setup previously described [26,34]. Samples were excited with the output of a Northern Lights tunable dye laser (Dakota Technologies, Inc.) through a potassium dihydrogen phosphate frequency-

doubling crystal. The dye laser was operated on LDS 698 laser dye (Exciton, Catalog No.06980), and it was pumped with the second harmonic of a 10-Hz Nd:YAG Q-switched solid-state laser (Big Sky Laser Technologies). Fluorescence was detected with a multichannel detector consisting of a front-illuminated intensified charge coupled device (ICCD) from Andor Technology. The minimum gate time of the intensifier was 2 ns. The CCD had the following specifications: active area, 690–256 pixels (26 mm^2 pixel size photocathode); dark current, 0.002 electrons/pixel/s; readout noise, 4 electrons at 20 kHz. The ICCD was mounted at the exit focal plane of a spectrograph (SPEX 270 M) equipped with a 1200 grooves mm^{-1} grating blazed at 500 nm. The system was used in the external trigger mode. The gating parameters (gate delay, gate width, and the gate step) were controlled with a digital delay generator (DG535, Stanford Research Systems, Inc.) via a GPIB interface. Custom LabView software (National Instruments) was developed in-house for complete instrumental control and data collection.

3.10. Time-resolved measurements

Wavelength time matrices (WTMs) and TREEMs were recorded using a 42 μm spectrograph slit-width. Time-resolved fluorescence spectra were recorded using a minimum delay of 10 ns, which was sufficient to avoid the need to consider convolution of the laser pulse with the analytical signal. Unless otherwise noted, each time-resolved spectrum corresponds to the accumulation of 100 laser pulses.

Fluorescence decays were obtained via a three-step procedure: (1) full sample and background WTM collection; (2) Background decay curve subtraction from the fluorescence decay curve at a wavelength of maximum emission for each metabolite; and (3) Fitting of the background corrected data to single-exponential decays. Commercial software (Origin; Microcal Software, Inc.) was used for curve fitting of fluorescence lifetimes. Fitted decay curves $y = y_0 + A_1 e^{[-(x - x_0)t]}_1$ are obtained by fixing x_0 and y_0 at a value of zero.

TREEMs were recorded using an excitation range (340–347 nm) common to the three studied metabolites. The tunable dye laser was stepped at 1 nm increments, generating a total of six (6) excitation wavelengths. Fluorescence was recorded within the 355–430 emission range using the following delay times (D):10 ns ($TREEM_1$ and $TREEM_2$), 50 ns ($TREEM_3$), 100 ns ($TREEM_4$) and 200 ns ($TREEM_5$). The gate widths (G) were as follows: 40 ns ($TREEM_1$), 120 ns ($TREEM_2$), 200 ns ($TREEM_3$) and 500 ns ($TREEM_4$ and $TREEM_5$). These parameters provided the following time windows (D-D + G) for TREEM collection: 10–50 ns ($TREEM_1$), 10–130 ns ($TREEM_2$), 50–250 ns ($TREEM_3$), 100–600 ns ($TREEM_4$) and 200–700 ns ($TREEM_5$).

3.11. Chemometric algorithms and software

All algorithms were implemented in MATLAB 7.10 [35]. A useful interface for data input and parameters setting written by Olivieri et al. [36], which can be downloaded from www.iquir-conicet.gov.ar/descargas/mvc3.rar, was employed for PARAFAC and U-PLS/RTL implementation.

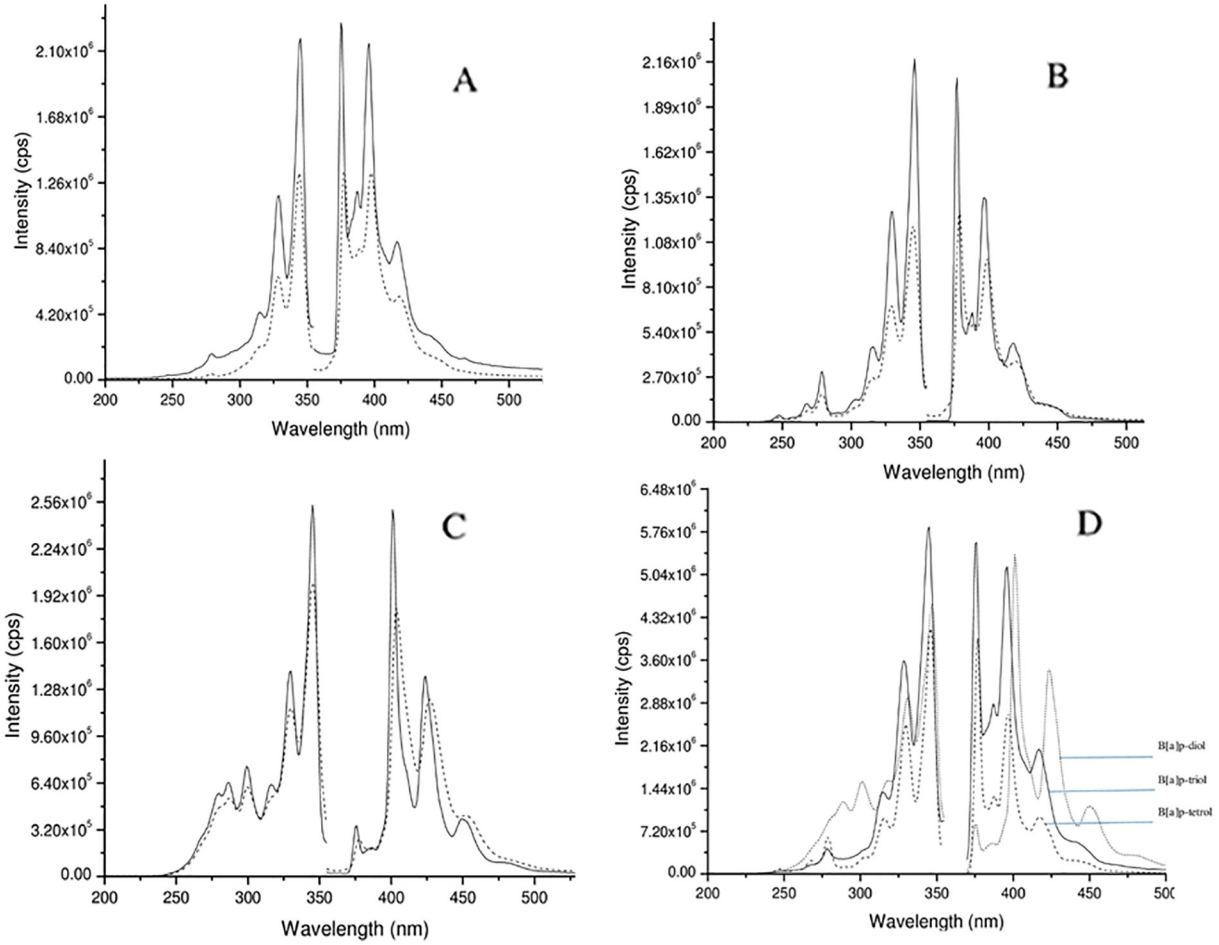

Fig. 1. Room temperature (dotted line) and (solid line) 77 K spectra of (A) B[*a*]P-tetrol, (B) B[*a*]P-triol and (C) B[*a*]P-diol. (D) 77 K overlaid spectra of B[*a*]P-diol (dotted line), B[*a*]P-triol (solid line) and B[*a*]P-tetrol (trace line). All spectra were recorded from C-18 membranes previously used to extract 10 mL of 20 ng mL^{-1} metabolite solution. Al spectra were recorded using a 2 nm excitation/emission bandpass.

4. Results and discussion

4.1. Spectral features of B[a]P metabolites at RT and 77 K

B[*a*]P-diol, B[*a*]P-triol and B[*a*]P-tetrol were selected for these studies as a representative examples of the rich and heterogeneous distribution of metabolic products produced by B[*a*]P. Previous studies in our lab [24] showed no significant changes in the room temperature (RT) spectra of these metabolites when recorded from pure standard solutions in 10% methanol-water (v/v), hydrolyzed urine samples and from the surface of SPE membranes. Fig. 1A–C compare the RT and 77 K excitation and fluorescence spectra of the three studied compounds adsorbed on C-18 membranes. All spectra were recorded with a commercial spectrofluorimeter and the FOP using a 2 nm excitation and emission band-pass. Lowering the temperature to 77 K did not change the spectral profiles of the studied metabolites but enhanced their fluorescence emission on extraction membranes. Reducing the sample temperature often increases fluorescence quantum yields and eliminates complications with oxygen quenching and energy transfer. In addition to the fluorescence enhancements, minor blue shifts were observed in the maximum emission wavelengths of the three compounds; namely 2 nm for B[*a*]P-diol and B[*a*]P-tetrol and 3 nm for B[*a*]P-triol. Fig.1D overlays the 77 K excitation and fluorescence spectra of the three metabolites on SPE membranes. Due to the strong spectral overlapping of excitation and fluorescence spectra, it is not possible to select an appropriate set of excitation and emission wavelengths for the accurate quantitation of any given metabolite.

4.2. Analytical figures of merit at RT and 77 K

Table 1 compares the RT and 77 K analytical figures of merit (AFOMs) of the three metabolites on SPE membranes. Fluorescence measurements were made with the aid of the laser system and the FOP at the maximum excitation and fluorescence wavelength of each metabolite. Standard solutions were prepared in human urine and hydrolyzed prior to SPE. In all cases, the volume of extracted sample was 10 mL and the mass of extracted metabolite did not surpass the nominal breakthrough mass (30 mg) of extraction membranes. Since metabolite elution is not required for quantitative analysis, the percentage of metabolite retained on the extraction membrane corresponds to the analytical recovery of the method. Within a confidence interval of 95%, all the analytical recoveries were statistically equivalent to 100% (N = 3). The linear dynamic ranges (LDRs) of the calibration curves were obtained with a minimum of five metabolite concentrations. No efforts were made to experimentally obtain the upper concentration limits of the calibration curves. Each intensity plotted in the calibration graph corresponds to the average signal recorded from three extraction membranes. Each membrane signal corresponds to the accumulation of 100 laser pulses. The correlation coefficients (R) close to unity indicate a linear relationship between metabolite concentrations and fluorescence intensity. Satisfactory results were also obtained by the ANOVA test suggested by IUPAC [37]. The limits of quantitation (LOQs) and the LODs were at the pg mL^{-1} concentration level. Although the fluorescence intensities of the studied metabolites were higher at 77 K than at RT, lowering the temperature did not improve the detection levels with the laser system. The main reason for the lack of LOQs and LODs improvements is the higher background signals of the extraction membranes at 77 K. Although the TLC treatment previous to membrane use considerably reduces the original fluorescence background, the residual signal of the membrane is enhanced by lowering the temperature to 77 K. Since the LOQs and LODs are based on the standard deviation of the residual signals, their values reflect the higher standard deviations of the residual signal averages at 77 K.

The detection levels obtained with the laser system are approximately two orders of magnitude better than the LOQs and LODs previously obtained with commercial instrumentation [24]. In our previous studies, [24] ng mL^{-1} detection levels were only achieved after submitting the SPE membranes to a dual background treatment procedure consisting of TLC followed by a computational step. The latter was carried out with the aid of Asymmetric Lest Squares (ALS), a smoothing algorithm originally devised for baseline correction of chromatographic data [38–40]. The application of this algorithm to the residual background signal of SPE membranes could certainly improve the LOQs and LODs obtained with laser-based instrumentation.

4.3. Fluorescence lifetimes of B[a]P metabolites at RT and 77 K

Pulsed excitation sources offer prospects for time-resolving the emission to improve signal-to-background ratios and reduce spectral interference. Multi-channel detectors can acquire emission spectra at good signal-to-noise much faster than is possible with a scanning monochromator. Collecting the entire emission spectrum at once avoids problems associated with pulse-to-pulse fluctuation, laser intensity drift, and photodecomposition that could degrade analytical figures of merit. Our group has shown that the combination of a pulsed tunable dye laser, a pulsed delay generator, a spectrograph, and an ICCD is well suited for the rapid collection of both WTMs and TREEMs [25,26,34]. A WTM consists of a series of emission spectra recorded under one excitation wavelength and different time delays after the laser excitation pulse. Recording WTMs during the fluorescence decay of the sample provides an additional parameter for fluorophore identification (lifetime). Unambiguous fluorophore identification is made possible on the basis of spectral and lifetime information. Fluorescence lifetimes also report on spectral peak purity, an essential condition for the accurate quantitation of analytes in complex fluorophore mixtures [25,32].

Table 2 compares the effect of lowering the temperature on the fluorescence lifetimes of the studied metabolites adsorbed on SPE membranes. Lowering the temperature to 77 K increased the fluorescence

Table 1
Analytical figures of merit of B[*a*]P metabolites obtained from SPE membranes at RT and 77 K.

B[*a*]P metabolite	λexc/λem[a] (nm)		SPE recovery[b] (%)	LDR[c] (ng·mL^{-1})		R[d]		LOQ[e] (ng.mL^{-1})		LOD[f] (ng·mL^{-1})	
	RT	77 K		RT	77 K	RT	77 K	RT	77 K	RT	77 K
B[*a*]P-diol	342/400	342/398	93.9 ± 3.5	0.03–40	0.02–40	0.9876	0.9822	0.03	0.02	0.01	0.006
B[*a*]P-triol	344/378	344/375	92.4 ± 3.8	0.02–40	0.02–40	0.9840	0.9883	0.02	0.01	0.006	0.003
B[*a*]P-tetrol	345/377	345/375	91.9 ± 4.1	0.05–40	0.02–40	0.9823	0.9677	0.05	0.02	0.02	0.005

[a] Excitation and emission wavelengths.
[b] SPE recovery = $(C_{AE} / C_{BE}) \times 100$; where C_{BE} and C_{AE} refer to the metabolite concentrations before and after extraction, respectively. Metabolite concentrations were obtained by measuring the room-temperature fluorescence signals of pure standards at medium linear concentrations. Each concentration is based on the average of three fluorescence measurements of three independent extractions (N = 9). Each reported recovery is based on six fluorescence measurements of six independent extractions (N = 18).
[c] LDR = linear dynamic range in ng·mL^{-1} extending from the limit of quantification (LOQ) to an arbitrarily chosen upper linear concentration.
[d] R = Correlation coefficient of calibration curve.
[e] Limit of quantitation calculated as $10 \times S_B / m$; where S_B is the standard deviation of 16 blank measurements and m is the slope of the calibration curve.
[f] Limit of detection calculated as $3 \times S_B / m$.

Table 2
Fluorescence lifetimes recorded from SPE at RT and 77 K.

Lifetimes (τ; ns)[a]	B[*a*]P-diol	B[*a*]P-triol	B[*a*]P-tetrol
RT	35.40 ± 1.90	132.01 ± 9.64	166.51 ± 1.85
77 K	43.88 ± 2.55	185.81 ± 4.24	221.32 ± 8.67

[a] Average fluorescence lifetimes (N = 3) recorded at the maximum excitation (λ_{exc}) and emission (λ_{em}) wavelengths. RT: $\lambda_{exc}/\lambda_{em}$ = 342/400 nm (B[*a*]P-diol), $\lambda_{exc}/\lambda_{em}$ = 344/378 nm (B[*a*]P-triol) and $\lambda_{exc}/\lambda_{em}$ = 345/377 (B[*a*]P-tetrol); 77 K: $\lambda_{exc}/\lambda_{em}$ = 342/398 nm (B[*a*]P-diol), $\lambda_{exc}/\lambda_{em}$ = 344/375 nm (B[*a*]P-triol) and $\lambda_{exc}/\lambda_{em}$ = 345/375 (B[*a*]P-tetrol).

lifetimes of the three metabolites. This phenomenon is in good agreement with the fluorescence enhancement observed at 77 K. In terms of rate constants (phtons.s^{-1}) of fluorescence emission (k_F) and non-radiative deactivation processes (k_{NR}) of the first singlet excited state S_1, the fluorescence quantum yield (ϕ_F) and the fluorescence lifetime (τ_F) of a fluorophore in the absence of an external quencher can be expressed as $\phi_F = k_F / k_F + k_{NR}$ and $\tau_F = 1 / k_F + k_{NR}$, respectively [26]. Since both ϕ_F and τ_F are inversely proportional to k_{NR}, lowering the temperature to 77 K appears to reduce the contribution of k_{NR} to the radiationless deactivation of S_1. The emission of phosphorescence at 77 K was not observed from any of the studied metabolites.

Fig. 2 displays the 77 K fluorescence decays recorded from SPE membranes at the maximum excitation and emission wavelengths of each metabolite. In all cases, single exponential decays were observed. The agreement between the calculated and observed points over the first two lifetimes of the decays agrees to within about 1% and the residuals show no systematic trends. Comparison of time scales suggests the possibility to selectively determine either B[*a*]P-tetrol or B[*a*]P-triol in the presence of B[*a*]P-diol. A time delay of 200 ns should be enough to time-discriminate the relatively short – lived emission of B[*a*]P-diol and avoid its spectral interference. Since the fluorescence decays of B[*a*]P-tetrol and B[*a*]P-triol extend over very similar time-windows, time discrimination of these two metabolites should be difficult to accomplish.

4.4. TREEM analysis

This fact is clearly depicted in Fig. 3. The three TREEMs were recorded at 77 K from a 10 mL urine sample extracted on an octadecyl membrane. Previous to extraction, the urine sample was spiked with the three metabolites and hydrolyzed according to the procedure described previously. The final concentration of each metabolite in the spiked sample was 1 ng·mL^{-1}. The time windows (D-D + G) for TREEM collection were 10–50 ns ($TREEM_1$), 50–250 ns ($TREEM_3$) and 200–700 ns ($TREEM_5$). Based on the time decay profiles of Fig. 2, $TREEM_1$ and $TREEM_3$ compound the spectral contribution of the three metabolites. Although the longer delay (200 ns) of $TREEM_5$ removes the contribution of B[*a*]P-diol from the data matrix, the resulting fluorescence still compounds the contributions of B[*a*]P-triol and B[*a*]P-tetrol.

When compared to the excitation spectra of the studied metabolites, the range of excitation wavelengths (340–347 nm) for TREEM collection is rather narrow. Since B[*a*]P-triol and B[*a*]P-tetrol metabolites show very similar spectral features (Fig. 1D), the possibility of selective excitation away from 340 to 347 nm does not exist. The only metabolite that could have benefitted from selective excitation is B[*a*]P-diol. In

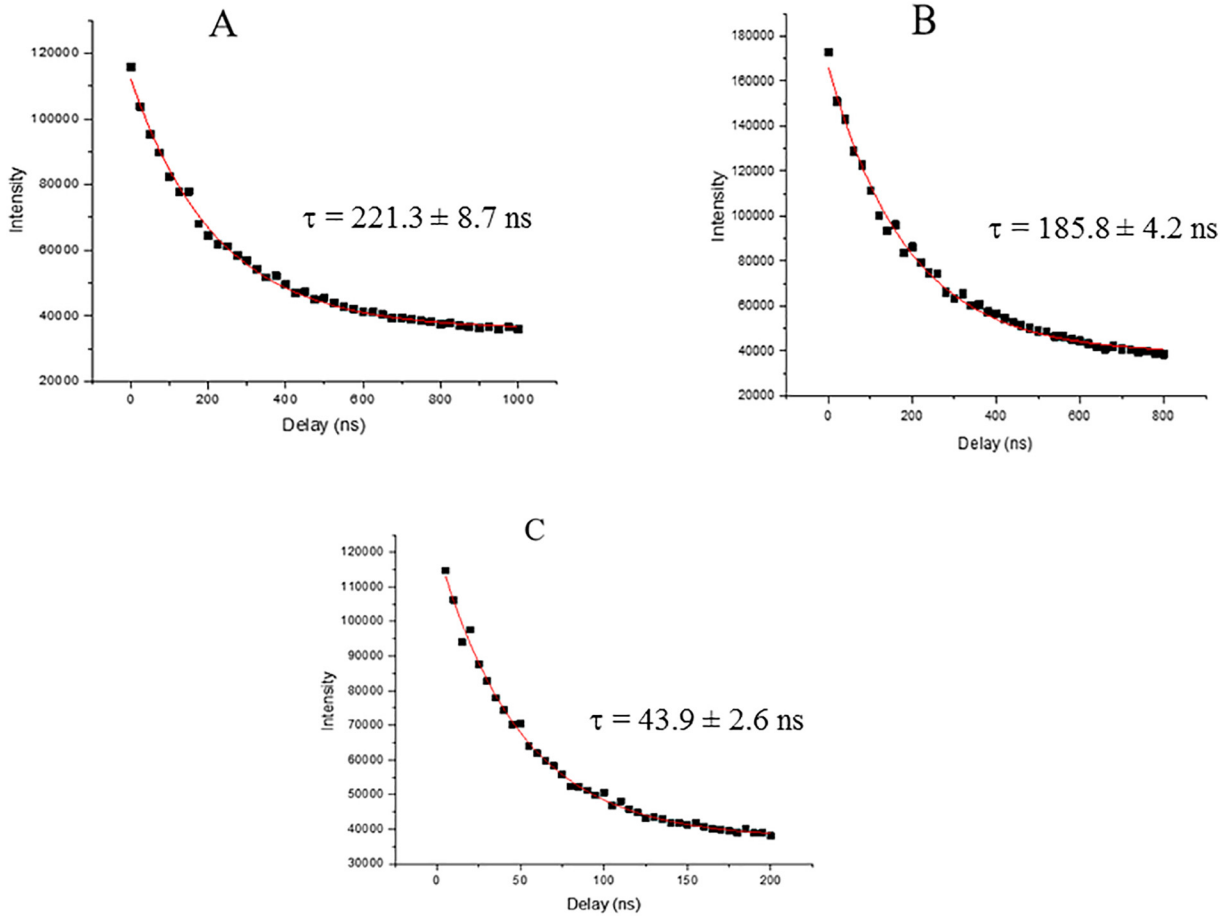

Fig. 2. 77 K fluorescence decays recorded from C-18 membranes previously used to extract 10 mL of 20 ng mL^{-1} standard solutions of (A) B[*a*]P-tetrol, (B) B[*a*]P-triol and (C) B[*a*]P-diol. Exponential decays were obtained at the maximum excitation and emission wavelengths of each metabolite using a 42 μm spectrograph slit width. τ = lifetime values obtained from the fitted decays.

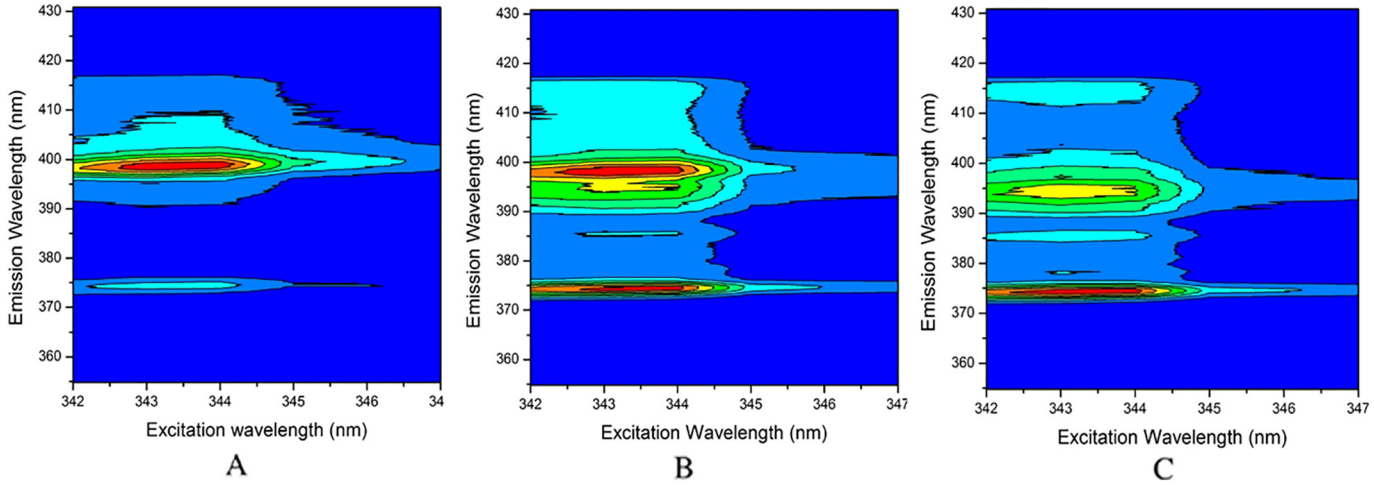

Fig. 3. 77 K TREEMs recorded from a C-18 membrane previously used to extract 10 mL of a 1 ng mL^{-1} aqueous mixture of B[*a*]P-diol, B[*a*]P-triol and B[*a*]P-tetrol. Time windows were as follows: (A) Delay = 10 ns, Delay + Gate = 40 ns; (B) Delay = 50 ns, Delay + Gate = 250 ns; (C) Delay = 200 ns, Delay + Gate = 700 ns. Excitation wavelength was stepped at 1.0 nm increments. Each emission spectrum corresponds to the accumulation of 100 laser pulses.

comparison to B[*a*]P-triol and B[*a*]P-tertol, B[*a*]P-diol shows stronger excitation features below 300 nm. TREEM collection within the ≈280–300 nm excitation range under relatively short delay and gate times could have enhanced the spectral features of B[*a*]P-diol over the other two metabolites. For reasons of operational simplicity – i.e. the use of a single laser dye with our tunable dye laser – this alternative was not attempted.

4.5. PARAFAC and U-PLS/RTL modeling

The first attempts to modeling TRECC data of B[*a*]P-diol, B[*a*]P-triol and B[*a*]P-tetrol were made with PARAFAC. This robust algorithm is well-known for its ability to calibrate tri-linear data efficiently [41]. PARAFAC modeling of the twelve pure standards and metabolites validation sample was carried out with thirteen TREECs generated with the following five time windows: 10–50 ns ($TREEM_1$), 10–130 ns ($TREEM_2$), 50–250 ns ($TREEM_3$), 100–600 ns ($TREEM_4$) and 200–700 ns ($TREEM_5$). Each resulting TREEC corresponded to a four-way array with the following size: $(I + 1 = 13) \times (J = 6) \times (K = 1024) \times (L = 5)$. The correct number of sample constituents (three) for the calibration set and validation samples was selected based on the so-called core consistency analysis (CORCONDIA). The non-negativity restriction was applied to all modes [42].

Fig. 4 shows the emission, excitation and time profiles obtained with PARAFAC for the three metabolites. Visual comparisons of the spectral profiles predicted by PARAFAC to the excitation and fluorescence spectra in Fig. 1 shows remarkable discrepancies between predicted and experimental data. The best prediction was obtained for B[*a*]P-diol, which shows an emission spectrum similar to the PARAFAC profile. Unacceptable results were also obtained for the time decay profiles extracted with PARAFAC. Accurate predictions should have led to exponential decays similar to those reported in Fig. 2. The inability of PARAFAC to deliver accurate predictions is a strong indication that the data arrays of the studied metabolites do not follow the quadrilinearity property [42].

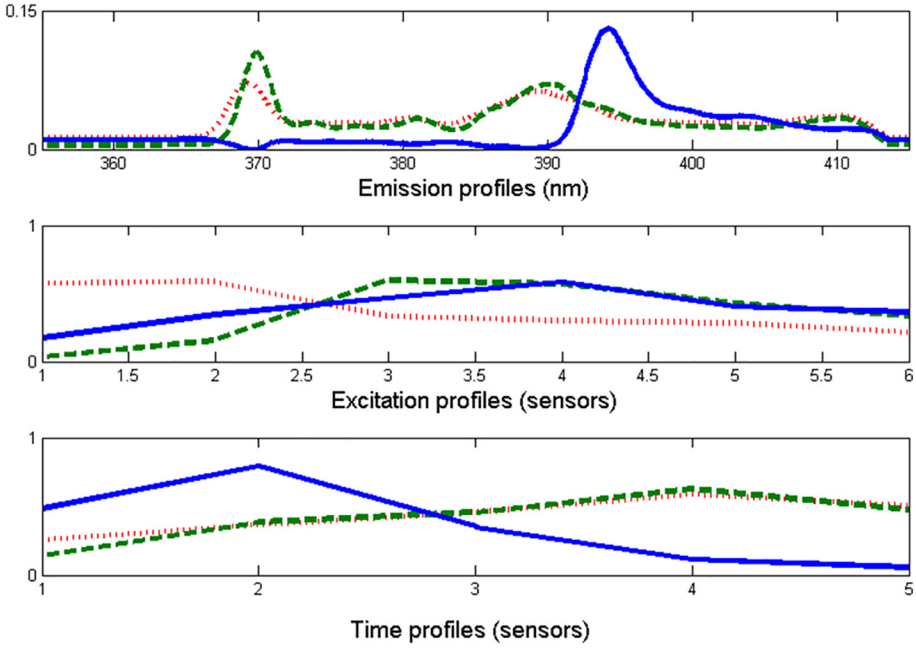

Fig. 4. PARAFAC modeling profiles obtained for B[*a*]P-diol (blue solid line), B[*a*]P-triol (green dashed line) and B[*a*]P-tetrol (red shot-dashed line). (For interpretation of the references to color in this figure legend, the reader is referred to the web version of this article.)

Table 3
Prediction results obtained from validation samples suing U-PLS/RTL modeling.

Sample	B[*a*]P-diol (ng mL^{-1})		B[*a*]P-triol (ng mL^{-1})		B[*a*]P-tetrol (ng mL^{-1})	
	Nominal	Predicted	Nominal	Predicted	Nominal	Predicted
1	1.00	0.97	1.00	1.05	0.25	0.20
2	0.70	0.72	0.70	0.74	0.70	0.60
3	0.03	0.04	0.70	0.80	0.70	0.65
4	0.62	0.60	0.03	0.02	0.62	0.70
5	0.23	0.22	0.23	0.26	1.00	0.95
6	1.00	0.96	0.23	0.28	0.23	0.18
7	0.62	0.63	0.62	0.58	0.03	0.04
8	1.00	1.04	0.23	0.17	1.00	1.08
9	0.62	0.60	0.62	0.61	1.20	1.28
10	0.62	0.64	0.62	0.71	0.62	0.58
11	0.62	0.61	1.20	1.30	0.62	0.57
12	0.23	0.20	0.23	0.20	0.23	0.30
13	1.20	1.25	0.62	0.65	0.62	0.70
14	0.23	0.24	1.00	1.05	1.00	1.10
15	1.00	1.03	1.00	1.10	1.00	1.05
16	0.23	0.20	1.00	0.96	0.23	0.30
REP (%)[a]		4.3		9.6		10.9
Recovery (%)[b]		101 ± 10		101 ± 14		106 ± 21

[a] REP = Relative error prediction; $REP = \frac{100}{c}\left[\frac{1}{I}\sum_1^I (cact - cpred)2\right]^{1/2}$, where I is the number of samples, c is the mean concentration, and c_{act} and c_{pred} are the actual and predicted concentrations, respectively.

[b] Recoveries represent the averages of 3 independent determinations (n = 3).

Among the more flexible approaches capable to cope with intrinsically more complex data [41], we chose U-PLS/RTL. The number of latent variables for the application of U-PLS/RTL was selected by the well-known leave-one-sample-out cross-validation procedure. The optimum number of factors was estimated by calculating the ratios $F(A) = \text{PRESS}(A < A^*) / \text{PRESS}(A^*)$, where $\text{PRESS} = \Sigma(y_{i,act} - y_{i,pred})^2$, A was the trial number of factors and A^* the one corresponding to the minimum PRESS. The number of selected factors led to a 75%-less probability that $F > 1$. Similar to PARAFAC, the latter procedure suggested three latent variables for the calibration of each metabolite.

Predicted concentrations on validation samples are depicted in Table 3. Since the validation samples did not contain interferences, their concentrations were predicted without the implementation of RTL. Despite the strong overlapping that exists among the three modes, the comparison of predicted and nominal concentrations confirms the ability of U-PLS to deliver accurate predictions in the absence of interference.

The prediction of metabolite concentrations in synthetic and real urine samples required the implementation of RTL. The number of potential interferences (N_i) was evaluated with Eq. 4. Since the final residuals (s_u) stabilized at $N_i = 2$ in both types of urine samples, two latent variables were adopted for the prediction of concentrations in all cases. Fig. 5 shows the spectral and time profiles of the predicted interference. The quantitative results are shown in Tables 4 and 5. The agreements among nominal and predicted values confirm the ability of U-PLS/RTL to deliver accurate predictions with only two latent variables.

Additional confirmation on the accuracy of U-PLS/RTL was obtained by applying the elliptic joint confidence region (EJCR) test to real urine samples [43]. The obtained results are shown in Fig. 6. The elliptical domains of the three metabolites include the theoretically predicted

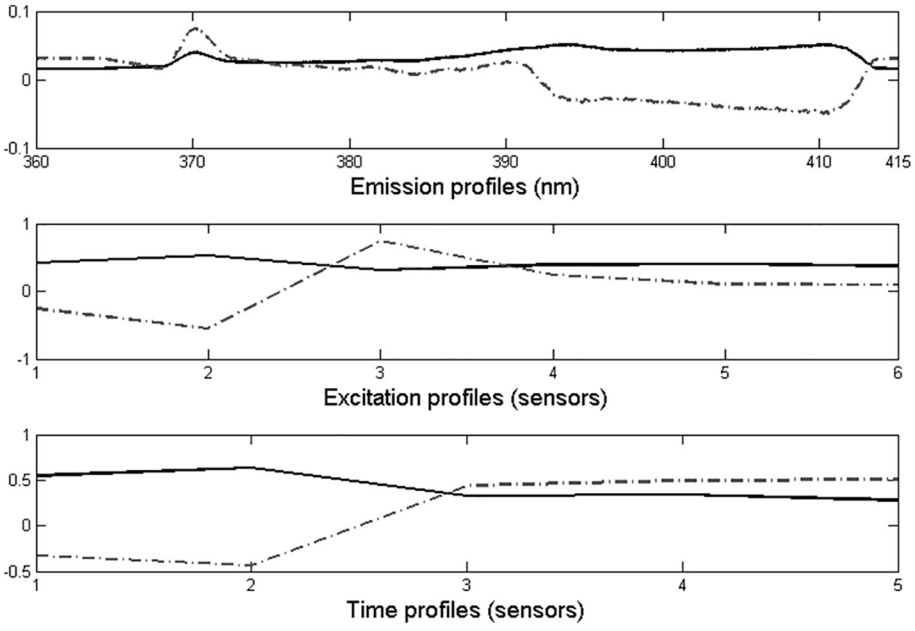

Fig. 5. Profiles corresponding to both RTL factors (non-model compounds present in the real urine sample, i.e. interference): (A) emission, (B) excitation, and (C) time. Solid line: first RTL factor, and dotted line: second RTL factor.

Table 4
U-PLS/RTL prediction results from synthetic urine samples spiked with the studied metabolites using 2 RTL factors to achieve the second-order advantage.

Sample	B[*a*]P-diol (ng mL^{-1})		B[*a*]P-triol (ng mL^{-1})		B[*a*]P-tetrol (ng mL^{-1})	
	Nominal	Predicted	Nominal	Predicted	Nominal	Predicted
1	1.00	0.96	1.00	1.04	0.25	0.21
2	0.70	0.71	0.70	0.75	0.7	0.62
3	0.03	0.04	0.70	0.79	0.7	0.64
4	0.62	0.59	0.03	0.020	0.62	0.71
5	0.23	0.25	0.23	0.27	1.00	0.96
6	1.0	0.95	0.23	0.26	0.23	0.19
7	0.62	0.63	0.62	0.56	0.03	0.03
8	1.0	1.03	0.23	0.17	1.00	1.10
9	0.62	0.61	0.62	0.60	1.20	1.15
10	0.62	0.65	0.62	0.70	0.62	0.65
11	0.62	0.60	1.20	1.31	0.62	0.65
12	0.23	0.22	0.23	0.18	0.23	0.29
13	1.20	1.24	0.62	0.65	0.62	0.71
14	0.23	0.23	1.00	1.06	1.00	1.11
15	1.00	1.04	1.00	1.08	1.00	0.94
16	0.23	0.20	1.00	1.05	0.23	0.28
REP (%)[a]		4.4		9.6		10.5
Recovery (%)[b]		101 ± 10		101 ± 13		104 ± 14

[a] REP = Relative error prediction; $REP = \frac{100}{c}\,[\frac{1}{I}\sum_1^I (cact - cpred)2]^{1/2}$, where I is the number of samples, c is the mean concentration, and c_{act} and c_{pred} are the actual and predicted concentrations, respectively.
[b] Recoveries represent the averages of 3 independent determinations (n = 3).

values of the slope (1) and intercept (0). Interesting to note is the better accuracy obtained for B[*a*]P-diol. Its red-shifted fluorescence spectrum (see Fig. 1D) and much shorter fluorescence decay (see fig. 2) appear to facilitate its determination in the presence of the other two metabolites.

The AFOMs in Table 2 were calculated with univariate statistics under ideal experimental conditions, i.e. with pure standard solutions in the absence of spectral interference. Table 6 provides a more realistic assessment of the AFOMs for the problem at hand as it considers the spectral interference from other fluorophores co-adsorbed on the extraction membranes. These include the three studied metabolites and the presence of unknown concomitants in the urine samples. The sensitivity of the method was calculated according to Eq. 6:

$$\mathrm{SEN}_n = \left\{ \mathbf{g}_n^{\mathrm{T}} \left[\mathbf{Z}_{\mathrm{exp}}^{\mathrm{T}} (\mathbf{I} - \mathbf{Z}_{\mathrm{unx}} \mathbf{Z}_{\mathrm{unx}}^{+}) \mathbf{Z}_{\mathrm{exp}} \right]^{-1} \mathbf{g}_n \right\}^{-1/2} \quad (6)$$

in which $\mathbf{g}_n^{\mathrm{T}}$ and $\mathbf{Z}_{\mathrm{exp}}^{\mathrm{T}}$ correspond to the $\mathbf{v}_{\mathrm{UPLS},n}$ vector of latent PLS coefficients and $\mathbf{P}_{\mathrm{UPLS}}$ matrix of U-PLS calibration loadings, respectively. $\mathbf{Z}_{\mathrm{unx}}$ can be computed from the profiles extracted by the RTL procedure for the unexpected constituents in the various data modes [44]. It should be noted that, when applying multi-way calibration methods, the SENn values become sample-specific. Thus, the results in Table 6 should be regarded as average values of the sets of samples we investigated and not as representative figures of the whole multivariate method. The inverse of the analytical sensitivity (γ^{-1}) was computed as the ratio between the instrumental noise (s_x) and the SENn value. s_x was computed from a sample of zero concentration. The limit of detection and quantification were calculated as LOD = 3.3 s_x/SENn and LOQ = 10 s_x/SENn [44]. Comparison to 77 K data in Table 2 shows no significant deterioration of the LOQ and LOD values in the presence of spectral interference.

5. Conclusion

Previous SPE-RTF reports on analysis of PAH metabolites in urine samples utilized commercial instrumentation with continues excitation

Table 5
U-PLS/RTL prediction results from real urine samples spiked with the studied metabolites using 2 RTL factors to achieve the second-order advantage.

Sample	B[*a*]P-diol (ng mL^{-1})		B[*a*]P-triol (ng mL^{-1})		B[*a*]P-tetrol (ng mL^{-1})	
	Nominal	Predicted	Nominal	Predicted	Nominal	Predicted
1	1.00	0.98	1.00	0.95	0.25	0.22
2	0.70	0.71	0.70	0.75	0.70	0.64
3	0.03	0.04	0.70	0.62	0.70	0.66
4	0.62	0.58	0.03	0.019	0.62	0.68
5	0.23	0.23	0.23	0.25	1.00	0.95
6	1.00	0.95	0.23	0.28	0.23	0.20
7	0.62	0.64	0.62	0.59	0.03	0.04
8	1.00	1.02	0.23	0.16	1.00	1.10
9	0.62	0.60	0.62	0.64	1.20	1.18
10	0.62	0.60	0.62	0.70	0.62	0.58
11	0.62	0.60	1.20	1.30	0.62	0.66
12	0.23	0.22	0.23	0.17	0.23	0.19
13	1.20	1.24	0.62	0.65	0.62	0.68
14	0.23	0.23	1.00	1.04	1.00	1.08
15	1.00	1.04	1.00	1.11	1.00	0.93
16	0.23	0.20	1.00	0.95	0.23	0.29
REP (%)[a]		4.2		9.7		8.8
Recovery (%)[b]		101 ± 10		98 ± 15		103 ± 19

[a] REP = Relative error prediction; $REP = \frac{100}{c}\,[\frac{1}{I}\sum_1^I (cact - cpred)2]^{1/2}$, where I is the number of samples, c is the mean concentration, and c_{act} and c_{pred} are the actual and predicted concentrations, respectively.
[b] Recoveries represent the averages of 3 independent determinations (n = 3).

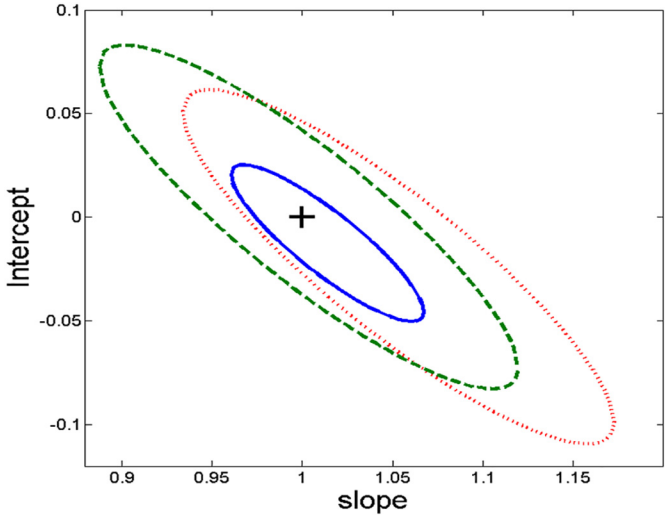

Fig. 6. Elliptic joint confidence region (EJCR) for the comparison of nominal and predicted concentrations of metabolites in real urine samples. Benzo[*a*]pyrene-*trans*-9,10-dihydrodiol (blue), benzo[*a*]pyrene-r-7,t-8,c-9-tetrahydrotriol (green dashed line) and benzo[*a*]pyrene-*r*-7,*t*-8,*c*-9,*c*-10-tetrahydrotetrol (red shot-dashed line). (For interpretation of the references to colour in this figure legend, the reader is referred to the web version of this article.)

sources [20–24]. Spectral overlapping from fluorescence concomitants in the sample matrix was addressed with the combination of RTF-EEMs and multivariate chemometric algorithms. The studies presented here utilized laser based instrumentation to record TREEMs at liquid nitrogen temperature. The entire experimental procedure consisted of two main steps, namely SPE of urine samples followed by TREEM collection at 77 K. A cryogenic FOP provided a simple and straightforward procedure for the measurement of samples at 77 K. TREEMs were rapidly recorded with the aid of a pulsed laser excitation source, a spectrograph and an ICCD. The entire experimental procedure took <10 min per sample.

Although the fluorescence intensities of the studied metabolites were higher at 77 K than at RT, lowering the temperature did not improve the detection levels with the laser system. The main reason for the lack of improvement was the higher background signals of the extraction membranes at 77 K. On the other end, the LODs obtained with the laser system (pg mL^{-1}) were approximately two orders of magnitude better than those previously reported with commercial instrumentation [20–24].

Lowering the temperature to 77 K did not improve the spectral resolution of the studied metabolites. Their fluorescence lifetimes became longer at 77 K but the lifetime differences remained approximately the same as those observed at RT. The accurate determination of B[*a*]P-diol, B[*a*]P-triol and B[*a*]P-tetrol provides strong evidence on the capability of U-PLS/RTL to handle strong spectral and lifetime overlapping.

Table 6
U-PLS/RTL analytical figures of merit of B[*a*]P metabolites obtained from C-18 membranes at 77 K.

B[*a*]P metabolite	SEN[a]	γ^{-1}, [b] (ng mL^{-1})	LOQ[c] (ng mL^{-1})	LOD[d] (ng mL^{-1})
B[*a*]P-diol	2.7×10^6	0.0039	0.035	0.012
B[*a*]P-triol	2.5×10^6	0.0043	0.048	0.013
B[*a*]P-tetrol	2.3×10^6	0.0046	0.042	0.014

[a–c] See text for explanation.

References

[1] J.T. Andresson, C. Achten, Time to say goodbye to the 16 EPA-PAHs? Toward an up-to-date use of PACs for environmental purposes, Polycycl. Aromat. Compd. 35 (2015) 330–354.
[2] J.B. Hochalter, Y. Zhong, S. Han, S. Carmella, S. Hecht, Quantitation of a minor enantiomer of phenanthrene tetraol in human urine: correlations with levels of overall phenanthrene tetraol, benzo[a]pyrene tetraol, and 1-hydroxypyrene, Chem. Res. Toxicol. 24 (2011) 262–268.
[3] Y. Zhong, S. Carmella, S. Balbo, Analysis of r-7,t-8,9,c-10-tetrahydroxy-7,8,9,10-tetrahydrobenzo[a]pyrene in human urine: a biomarker for directly assessing carcinogenic polycyclic aromatic hydrocarbon exposure plus metabolic activation, Chem. Res. Toxicol. 24 (2011) 73–80.
[4] S.S. Hecht, S.G. Carmella, P.W. Villalta, J.B. Hochalter, Analysis of phenanthrene and benzo[a]pyrene tetraol enantiomers in human urine: relevance to the bay region diol epoxide hypothesis of benzo[a]pyrene carcinogenesis and to biomarker studies, Chem. Res. Toxicol. 23 (2010) 900–908.
[5] X. Xu, J. Zhang, L. Zhang, W. Liu, C.P. Weisel, Selective detection of monohydroxy metabolites of polycyclic aromatic hydrocarbons in urine using liquid chromatography/triple quadrupole tandem mass spectrometry, Rapid Commun. Mass Spectrom. 18 (2004) (299–08).
[6] M. Bouchard, C. Viau, Urinary excretion kinetics of pyrene and benzo(a)pyrene metabolites following intravenous administration of the parent compounds or the metabolites, Toxicol. Appl. Pharmacol. 139 (1996) 301–309.
[7] W. Lee, H. Shin, J.E. Hong, H. Pyo, Y. Kim, Studies on the analysis of benzo(a)pyrene and its metabolites in biological samples by using high performance liquid chromatography/fluorescence detection and gas chromatography/mass spectrometry, Bull. Kor. Chem. Soc. 24 (2003) 559–565.
[8] Y. Wang, W. Zhang, Y. Dong, Quantification of several monohydroxylated metabolites of polycyclic aromatic hydrocarbons in urine by high-performance liquid chromatography with fluorescence detection, Anal. Bioanal. Chem. 383 (2005) 804.
[9] L. Kuusimaki, Y. Peltonen, P. Mutanen, K. Peltonen, K. Savela, Urinary hydroxy-metabolites of naphthalene, phenanthrene and pyrene as markers of exposure to diesel exhaust, Int. Arch. Occup. Environ. Health 77 (2004) 23–30.
[10] H. Wang, W.B. Wilson, A.D. Campiglia, Using gold nanoparticles to improve the recovery and the limits of detection for the analysis of monohydroxy-polycyclic aromatic hydrocarbons in urine samples, J. Chromatogr. A 385 (2009) 249.
[11] A. Likhachev, D. Beniashvili, K. Bykov, O. Kazanova, N. Loktionova, M. Tyndyk, O.S. Yatsuk, V. Yermilov, M. Zabezhinski, Biomarkers of individual susceptibility to carcinogens: application for biological monitoring, Int. Arch. Occup. Environ. Health 65 (1993) 155–158.
[12] A. Weston, R. Santella, E. Bowman, Detection of polycyclic aromatic hydrocarbon metabolites in urine from coal tar treated psoriasis patients and controls, Polycycl. Aromat. Compd. 5 (1994) 241–247.
[13] A.D. Campiglia, T. Vo-Dinh, Fiber optic sensor for laser-induced room-temperature phosphorescence detection of polycyclic aromatic compounds, Talanta 43 (1996) 1805–1814.
[14] E.D. Hagestuen, A.D. Campiglia, Phosphorimetric detection of polycyclic aromatic hydrocarbons on solid-phase extraction membranes, Appl. Spectrosc. 52 (1998) 1092–1102.
[15] A.F. Arruda, A.D. Campiglia, Determination of trace levels of polychlorinated biphenyls on reversed phase octadecyl bonded silica membranes, Anal. Chim. Acta 386 (1999) 271–280.
[16] A.F. Arruda, A.D. Campiglia, Screening potential of solid-phase extraction room temperature phosphorimetry for the analysis of polychlorinated dibenzofurans in water samples, Environ. Sci. Technol. 34 (2000) (4988–2000).
[17] E.D. Hagestuen, A.F. Arruda, A.D. Campiglia, On the improvement of solid-phase extraction room-temperature phosphorimetry for the analysis of polycyclic aromatic hydrocarbons in water samples, Talanta 52 (2000) 727–737.
[18] J.L. Whitcomb, A.D. Campiglia, Screening potential of solid-phase extraction and solid surface room temperature fluorimetry for polycyclic aromatic hydrocarbons in water samples, Talanta 55 (2001) 509–518.
[19] A.F. Arruda, H.C. Goicoechea, M. Santos, A.D. Campiglia, A.C. Olivieri, Solid—liquid extraction room temperature phosphorimetry and pattern recognition for screening polycyclic aromatic hydrocarbons and polychlorinated biphenyls in water samples, Environ. Sci. Technol. 37 (2003) 1385–1391.
[20] K. Vatsavai, H.C. Goicoechea, A.D. Campiglia, Direct quantification of monohydroxy-polycyclic aromatic hydrocarbons in synthetic urine samples via solid-phase extraction–room-temperature fluorescence excitation–emission matrix spectroscopy, Anal. Biochem. 376 (2008) 213–222.
[21] K. Calimag-Williams, H.C. Goicoechea, A.D. Campiglia, Room-temperature fluorescence spectroscopy of monohydroxy metabolites of polycyclic aromatic hydrocarbons on octadecyl extraction membranes, Talanta 85 (2011) 1805–1811.
[22] H.C. Goicoechea, K. Calimag-Williams, A.D. Campiglia, Multi-way partial least-squares and residual bi-linearization for the direct determination of monohydroxy-polycyclic aromatic hydrocarbons on octadecyl membranes via room-temperature fluorescence excitation emission matrices, Anal. Chim. Acta 717 (2012) 100–109.
[23] K. Calimag-Williams, G. Knobel, H.C. Goicoechea, A.D. Campiglia, Achieving second order advantage with multi-way partial least squares and residual bi-linearization with total synchronous fluorescence data of monohydroxy–polycyclic aromatic hydrocarbons in urine samples, Anal. Chim. Acta 811 (2014) 60–69.
[24] B. Alfarhani, M. Al-tameemi, A.V. Schenone, H.C. Goicoechea, F. Barbosa, A.D. Campiglia, Room temperature fluorescence spectroscopy of benzo[a]pyrene metabolites on octadecyl extraction membranes, Microchem. J. 129 (2016) 83–89.

[25] S. Yu, A.D. Campiglia, Direct determination of dibenzo [a, l] pyrene and its four dibenzopyrene isomers in water samples by solid—liquid extraction and laser-excited time-resolved Shpol'skii spectrometry, Anal. Chem. 77 (2005) 1440–1447.
[26] A.D. Campiglia, A.J. Bystol, S. Yu, Instrumentation for multidimensional luminescence spectroscopy and its application to low-temperature analysis in Shpol'skii matrixes and optically scattering media, Anal. Chem. 78 (2006) 484–492.
[27] H.C. Goicoechea, S. Yu, A.F. Moore, A.D. Campiglia, Four-way modeling of 4.2 K time-resolved excitation emission fluorescence data for the quantitation of polycyclic aromatic hydrocarbons in soil samples, Talanta 101 (2012) 330–336.
[28] C.M. Andersen, R. Bro, Practical aspects of PARAFAC modeling of fluorescence excitation-emission data, J. Chemom. 17 (2003) 200–215.
[29] R. Bro, PARAFAC. Tutorial and applications, Chemom. Intell. Lab. Syst. 38 (1997) 149–171.
[30] S. Wold, P. Geladi, K. Esbensen, J. Øhman, Multi-way principal components-and PLS-analysis, J. Chemom. 1 (1987) 41–56.
[31] J.A. Arancibia, A.C. Olivieri, D. Bohoyo Gil, A. Espinosa Mansilla, I. Durán Merás, A. Muñoz de la Peña, Trilinear least-squares and unfolded-PLS coupled to residual trilinearization: new chemometric tools for the analysis of four-way instrumental data, Chemom. Intell. Lab. Syst. 80 (2006) 77–86.
[32] H. Wang, A.D. Campiglia, Direct determination of benzo [a] pyrene in water samples by a gold nanoparticle-based solid phase extraction method and laser-excited time-resolved Shpol'skii spectrometry, Talanta 83 (2010) 233–240.
[33] A.F. Moore, H.C. Goicoechea, F. Barbosa Jr., A.D. Campiglia, Parallel factor analysis of 4.2 K excitation–emission matrices for the direct determination of dibenzopyrene isomers in coal-tar samples with a cryogenic fiber-optic probe coupled to a commercial spectrofluorimeter, Anal. Chem. 87 (2015) 5232–5239.
[34] A.D. Campiglia, S. Yu, A.J. Bystol, H. Wang, Measuring scatter with a cryogenic probe and an ICCD camera: recording absorption spectra in Shpol'skii matrixes and fluorescence quantum yields in glassy solvents, Anal. Chem. 7 (9) (2007) 1682–1689.
[35] MATLAB 7.10 (R2010a), The Math Works, Natick, MA, 2010.
[36] A.C. Olivieri, H.L. Wu, R.Q. Yu, MVC3: a MATLAB graphical interface toolbox for third-order multivariate calibration, Chemom. Intell. Lab. Syst. 116 (2012) 9–16.
[37] K. Danzer, L.A. Currie, Commission gen aspects analyt, Pure Appl. Chem. 70 (1998) 993–1014.
[38] P.H. Eilers, Parametric time warping, Anal. Chem. 76 (2004) 404–411.
[39] M.M. Galera, M.G. Garcia, M.J. Calzoni, H.C. Goicoechea, Determination of pharmaceuticals in river water by column switching of large sample volumes and liquid chromatography–diode array detection, assisted by chemometrics: an integrated approach to green analytical methodologies, J. Chromatogr. A 1217 (2010) 2042–2049.
[40] H.C. Goicoechea, M.J. Culzoni, M.G. García, M.M. Galera, Chemometric strategies for enhancing the chromatographic methodologies with second-order data analysis of compounds when peaks are overlapped, Talanta 83 (2011) 1098–1107.
[41] G.M. Escandar, H.C. Goicoechea, A. Muñoz de la Peña, A.C. Olivieri, Second and higher order data generation and calibration: a tutorial, Anal. Chim. Acta 806 (2014) 8–26.
[42] R. Bro, H.A.L. Kiers, a new efficient method for determining the number of components in PARAFAC models, J. Chemom. 17 (2003) 274–286.
[43] R. Jordi, F.X. Rius, Method comparison using regression with uncertainties in both axes, Trends Anal. Chem. 16 (1997) 211–216.
[44] A.C. Olivieri, G.M. Escandar, Practical Three-Way Calibration, Elsevier, Waltham, USA, 2014.